6916 *Biochemistry* **2010,** *49,* 6916–6927
DOI: 10.1021/bi100383m

BIOCHEMISTRY
including biophysical chemistry & molecular biology
Article

Investigation of Stability and Disulfide Bond Shuffling of Lipid Transfer Proteins by Molecular Dynamics Simulation[†]

Jane R. Allison, Gian-Peider Moll, and Wilfred F. van Gunsteren*

Laboratory of Physical Chemistry, Swiss Federal Institute of Technology ETH, 8093 Zürich, Switzerland

Received March 12, 2010; Revised Manuscript Received June 22, 2010

ABSTRACT: Proteins comprising each of the two plant nonspecific lipid transfer protein (LTP) families, LTP1s and LTP2s, share similar folds and biological functions and are stabilized by four native disulfide bonds. Disulfide-scrambling experiments suggested that rice LTP2 is more thermostable than rice LTP1 and identified multiple disulfide-scrambled isomers for LTP1 but only one for LTP2. According to the potential energy evaluated in two GROMOS force fields, however, rice LTP1 is more stable than either rice or wheat LTP2. Moreover, the published rice LTP2 NMR model structure is found to be highly unfavorable. The reasons for this are investigated, and it is found that the rice LTP2 sequence is in fact more compatible with the more ordered X-ray structure of wheat LTP2 than with the published rice LTP2 NMR model structure. The proposed disulfide bond shuffling of rice LTP1, rice LTP2, and, for comparative purposes, wheat LTP2 and a homology model combining the rice LTP2 sequence with the wheat LTP2 structure is then investigated with a computational disulfide-scrambling technique.

The plant nonspecific lipid transfer proteins (LTPs)[1] bind to a variety of lipids and transfer phospholipids between membranes in vitro (*1*, *2*). The two subfamilies of LTPs (*2*, *3*), LTP1 and LTP2, share about 30% sequence homology. The locations of hydrophobic and key positively charged residues and the eight cysteines that form disulfide bonds are well conserved both within and between the subfamilies. Proteins within a given subfamily have almost identical structures. There is also similarity in the overall structure between the two subfamilies (*4*, *5*), albeit to a lesser extent, as LTP1 proteins have four α-helices whereas LTP2 subfamily members have five short helices. Interestingly, the positions of the four disulfide bridges superimpose well despite the different pair patterns of the two subfamilies. Proteins from both subfamilies are capable of binding two lipid molecules, but those of the LTP1 subfamily bind them head to tail in a long, tunnel-like cavity (*6*) whereas LTP2 members bind them in two adjacent hydrophobic cavities (*7*).

The stability and unfolding behavior of rice LTP1 and LTP2 have been studied using the so-called disulfide-scrambling technique, in which proteins are subjected to various denaturants in the presence of a thiol catalyst (*8*−*16*). The disulfide-bonding patterns of the resulting scrambled isomers are determined by proteolysis followed by separation of the resulting peptides by HPLC. The isolated peptides are identified by sequence analysis and mass spectroscopy.

Recently, a simple molecular dynamics (MD) method for reproducing the experimental disulfide-scrambling conditions in silico (DS-MD) was proposed (*17*). The native disulfide bonds are not constrained, and the cysteine residues are neutralized to mimic the effects of a thiol catalyst. The simulations are run at high temperatures, as well as at room temperature, to replicate the conditions of thermal denaturation experiments.

In the disulfide-scrambling experiments (*16*), rice LTP2 was observed to be more stable than LTP1 in the presence of a thiol catalyst. LTP2 unfolds and refolds in an almost two-state manner, whereas LTP1 unfolds and refolds via identifiable partially folded intermediates with different disulfide-bonding patterns. As a result, parallels were drawn between LTP1/LTP2 and lysozyme/α-lactalbumin (LYS/αLA). Despite many similarities in their sequence and structure, both pairs of proteins exhibit different folding and unfolding behavior. LYS and αLA have also been subjected to disulfide-scrambling experiments (*11*−*13*), and αLA was previously studied using DS-MD.

Here, the stabilities of structures of rice LTP1 and rice and wheat LTP2 determined using X-ray crystallography or NMR spectroscopy are compared. The NMR model structures, particularly that of rice LTP2, are energetically less favorable than those determined by X-ray crystallography. Possible reasons for this are explored by detailed comparisons of the published structures and their dynamic changes during MD and DS-MD simulations. In comparison to the experimental results, LTP2 is structurally less stable during MD simulations than LTP1. The DS-MD simulations are then analyzed in terms of the proposed disulfide bond shuffling. Little evidence of the shuffling observed experimentally is found, suggesting that it may be an artifact of the experimental disulfide bond identification procedure.

METHODS

Simulation Setup. All simulations were performed using the GROMOS biomolecular simulation software (*18*) and the 45A4 or 53A6 GROMOS force field (*19*, *20*). Each protein was

[†]This work was supported by the National Center of Competence in Research (NCCR) in Structural Biology and by Grant 200020-121913 of the Swiss National Science Foundation.

*To whom correspondence should be addressed. E-mail: wfvgn@igc.phys.chem.ethz.ch. Phone: +41 44 632 5501. Fax: +41 44 632 1039.

[1]Abbreviations: LTP, lipid transfer protein; HPLC, high-performance liquid chromotography; MD, molecular dynamics; DS-MD, disulfide-scrambling MD; SS-MD, MD with disulfide bonds constrained; LYS, lysozyme; αLA, α-lactalbumin; NMR, nuclear magnetic resonance; PDB, Protein Data Bank; SPC, simple point charge; rmsd, root-mean-square deviation; rmsf, root-mean-square fluctuation; r_{gyr}, radius of gyration; E_{pot}, total potential energy; vdw, van der Waals; BMRB, BioMagResBank; GdmCl, guanidinium chloride; GdmSCN, guanidinium thiocyanate; ASA, accessible surface area; f_{VOL}, fractional volume; b_{VOL}, buried volume.

 Published on Web 07/14/2010

simulated with the native disulfide bonds constrained (SS-MD) and with DS-MD, in which all native disulfide bond-length constraints and the corresponding bond angle and dihedral angle potential energy terms are removed from all cysteines, resulting in neutral cysteine side chains.

Initial coordinates of the proteins were taken from the X-ray crystallographic or NMR model structures deposited in the PDB with entry codes 1rzl (*21*), 1bv2 (*22*), 1l6h (*4*), 1tuk (*7*), and 1n89 (*5*). The name used to refer to each, along with details of the structure determination method and the origin of the protein, is given in Table 1. Hydrogens were added using the GROMOS++ gch program. For LTP2, a homology model of the 1l6h (rice) sequence on the 1tuk (wheat) structure (R-LTP2-H) was created using the I-TASSER server (*23*). In the simulations, the protonation state of the ionizable residues was chosen according to the pH (8.4) at which the denaturation experiments on rice LTP1 and LTP2 were carried out (*16*). Each protein was subjected to 2000 steps of steepest descent energy minimization in the GROMOS force field. 1l6h was then solvated in a truncated octahedral box and 1rzl, 1bv2, 1tuk, and R-LTP2-H were solvated in rectangular boxes with a minimum distance of 1.2 nm from any solute atom to the edge of the box. The simple point charge (SPC) (*24*) water model was used, and periodic boundary conditions were applied. All simulations were initiated with the following equilibration scheme: first, the initial velocities were randomly generated from a Maxwell−Boltzmann distribution at 60 K. All solute atoms were restrained to their positions in the corresponding energy-minimized X-ray or NMR model structure through a harmonic potential energy term with a force constant of 2.5×10^4 kJ·mol^{-1} nm^{-2}. The system was simulated with these settings for 20 ps, followed by three consecutive 20 ps simulations; prior to each, the temperature was raised by 60 K, and the force constant for the positional restraints was reduced by a factor of 10. The position restraints were then removed, and four further 20 ps simulations were carried out, raising the temperature to 298, 328, 348, and 373 K. The final structure saved at each temperature was used as the starting configuration for a 10 ns production run at that temperature.

Table 1: Name, PDB Code, Source, Type of LTP, Number of Residues (N_{res}), and Structure Determination Method of the LTPs Studied in This Work

name	PDB code	source	type	N_{res}	method
R-LTP1-X	1rzl	rice	LTP1	91	X-ray
R-LTP1-N	1bv2	rice	LTP1	91	NMR
R-LTP2-N	1l6h	rice	LTP2	69	NMR
W-LTP2-X	1tuk	wheat	LTP2	67	X-ray
W-LTP2-N	1n89	wheat	LTP2	67	NMR

The SHAKE algorithm (*25*) was used with a geometric precision of 10^{-4} nm to constrain bond lengths, allowing for an integration time step of 2 fs. The center of mass motion was removed every 1000 time steps. The temperature and atmospheric pressure were kept constant using a weak coupling approach (*26*) with relaxation times $\tau_T = 0.1$ ps and $\tau_p = 0.5$ ps and an isothermal compressibility of 4.575×10^{-4} (kJ·mol^{-1} nm^{-3})$^{-1}$. Nonbonded interactions were calculated using a triple-range cutoff scheme. The interactions within a cutoff distance of 0.8 nm were calculated at every step from a pair list which was updated every fifth time step. At this point, interactions between atoms (of charge groups) within 1.4 nm were also calculated and were kept constant between updates. To account for the influence of the dielectric medium outside the cutoff sphere of 1.4 nm, a reaction field force based on a relative dielectric permittivity ε of 61 (*27*) was added.

Analysis. Potential energies were calculated according to the GROMOS 45A4 and 53A6 force fields. The atom-positional root-mean-square deviation (rmsd) between the indicated atoms of two structures was calculated after superposition of the indicated atoms. The root-mean-square-fluctuations (rmsf) of the C_α atoms of the backbone were calculated after superposition of the heavy atoms of the backbone. The radius of gyration (r_{gyr}) was computed for the heavy atoms of the backbone only. Secondary structure of each protein was assigned according to the rules defined by Kabsch and Sander's DSSP program (*28*). Disulfide bridges were considered to be formed if the sulfur−sulfur distance was less than 0.5 nm.

Software. All simulations and energy minimizations were carried out using MD++ 0.3.0 of the GROMOS05 package (*18*). For analysis, GROMOS++ 0.3.1 (*18*) was used. Additional analysis, conversion, and batch programs were written in Python or shell scripted. Visualization was done with the Visual Molecular Dynamics (VMD) (*29*) software. The proton chemical shifts were back-calculated using the SHIFTX (*30*) online server with default settings. Prior to chemical shift calculation, hydrogens were added to the homology model using the program REDUCE with side-chain rotations disabled (*31*). The quality of the NMR, X-ray and homology-modeled structures of LTP2 was checked using the programs VADAR (*32*) and PROCHECK (*33*), run using default settings on online servers.

RESULTS AND DISCUSSION

Stability of Native LTP1 and LTP2 Structures. Comparing the potential energy (E_{pot}) of the native structures of rice LTP1 solved by X-ray crystallography (*21*) (R-LTP1-X; see Table 1) and NMR spectroscopy (*22*) (R-LTP1-N) shows that R-LTP1-X is the most favorable in both GROMOS force fields (Table 2). In contrast, the E_{pot} of the NMR model structure of

Table 2: Contributions to the Potential Energy (kJ·mol^{-1}) of the Disulfide-Bonded X-ray and NMR Model Structures of Rice LTP1 Evaluated Using the GROMOS 53A6 or 45A4 Force Fields[a]

		bonded					nonbonded			
protein	force field	bonds	bond angles	improper dihedrals	proper dihedrals	total	van der Waals	electrostatic	total	total
R-LTP1-X	53A6	318	1012	28	374	1731	−3191	−6253	−9446	−7715
	45A4	318	1012	28	374	1714	−3904	−5123	−9027	−7296
R-LTP1-N	53A6	674	483	5	814	1975	−649	−7063	−7712	−5737
	45A4	674	483	5	814	1975	−1755	−5929	−7684	−5709

[a]Reference *19*.

Table 3: Contributions to the Potential Energy (kJ·mol^{-1}) of the Disulfide-Bonded X-ray and NMR Model Structures of Rice and Wheat LTP2 Evaluated Using the GROMOS 53A6 or 45A4 Force Fields[a] before and after Energy Minimization[b]

		bonded					nonbonded			
protein	force field	bonds	bond angles	improper dihedrals	proper dihedrals	total	van der Waals	electrostatic	total	total
R-LTP2-N	53A6	484	841	126	698	2148	3666	−2421	1246	3394
	45A4	484	840	126	698	2147	2233	−1841	392	2539
W-LTP2-X	53A6	427	873	30	298	1629	−1994	−4954	−6948	−5319
	45A4	427	873	30	298	1629	−2623	−4004	−6627	−4998
W-LTP2-N	53A6	241	228	8	641	1117	52	−2736	−2684	−1568
	45A4	240	228	8	641	1116	−779	−2263	−3043	−1926
R-LTP2-H	53A6	1757	953	18	273	3000	421959	−3892	418068	421068
	45A4	1757	950	18	273	2998	419042	−3037	416005	419003
after energy minimization										
		bonded					nonbonded			
protein	force field	bonds	bond angles	improper dihedrals	proper dihedrals	total	van der Waals	electrostatic	total	total	rmsd
R-LTP2-N	53A6	0	604	332	62	156	−2000	−3917	−5917	−4362	0.033
	45A4	0	514	206	578	1298	−2719	−2708	−5427	−4129	0.033
W-LTP2-X	53A6	0	373	110	281	763	−3251	−6162	−9413	−8649	0.011
	45A4	0	315	86	272	672	−3762	−4867	−8628	−7956	0.012
W-LTP2-N	53A6	0	489	147	475	1111	−2892	−6277	−9168	−8057	0.048
	45A4	0	370	120	461	952	−3303	−4083	−7386	−6434	0.032
R-LTP2-H	53A6	0	398	122	294	814	−2692	−5302	−7995	−7180	0.025
	45A4	0	335	98	277	712	−3057	−3839	−6897	−6185	0.019

[a]Reference *19*. [b]The rmsd (nm) of the backbone atoms (C, CA, N) between the starting and minimized structures are given in the final column of the lower half of the table.

rice LTP2 (*4*) (R-LTP2-N) is large and positive in both force fields (Table 3). The reasons for the extremely unfavorable energy of this model are discussed further below. Unfortunately, there is no X-ray structure of rice LTP2 with which to draw comparisons, so as a point of reference, wheat LTP2, which shares 60% sequence homology with rice LTP2 and whose structure has been solved by both X-ray crystallography (*7*) (W-LTP2-X) and NMR (*5*) (W-LTP2-N), is also considered. Only the results for the first (most representative) of the NMR model structures of wheat LTP2 are given unless otherwise specified. The E_{pot} of both wheat LTP2 structures is negative, although as for rice LTP1, the NMR model structure is the least favorable.

By considering the individual terms comprising the E_{pot}, also shown in Table 2 and Table 3, the aspects of the NMR structures responsible for their reduced stability may be isolated. The contributions to the covalent energy of the two rice LTP1 structures differ, but the total covalent energy is similar; thus the less favorable E_{pot} of R-LTP1-N stems from the noncovalent term, specifically, the much less negative van der Waals (vdw) term. The same is true for wheat LTP2, except that W-LTP2-N also has a less negative electrostatic term than the X-ray structure in both force fields. For R-LTP2-N, almost all of the covalent terms are more positive than the corresponding terms for W-LTP2-N or W-LTP2-X and the electrostatic energy is similar to that of W-LTP2-N. The crucial difference, however, is the large and positive vdw term, which dominates the total E_{pot} of R-LTP2-N due to its magnitude.

For the remainder of the structures, the unfavorable nature of some of the energy terms and the variation in E_{pot} between the structures may simply be due to differences between the force fields or energy functions used to determine each structure and the GROMOS force fields used here. In this respect, it is interesting to note that the mean total potential energy of the ensemble of 10 wheat LTP2 NMR model structures in the force field in which they were determined (*5*) is given as 515 kJ·mol^{-1} and the "E_{total} measure from Xplor" of rice LTP2, for which 15 structures were determined, is reported (*16*) to be 300 kJ·mol^{-1}. In comparison, W-LTP2-N has a negative E_{pot} in the GROMOS force fields whereas R-LTP2-N is significantly less favorable. There are clearly some differences, therefore, between the force fields used for the structure determination and the GROMOS force fields.

To eliminate the effect of small differences in covalent and vdw parameters between different force fields, the E_{pot} of each LTP2 structure was recalculated after minimization in the corresponding GROMOS force field (Table 3). Each of the covalent terms for a given structure is affected differently by the minimization, reflecting the fact that some aspects of the force field used to determine each structure differ from the GROMOS force fields more than others. Minimization reduces the total covalent energy for all structures. The electrostatic term also decreases for all systems, with W-LTP2-N undergoing the greatest change. Perhaps the most striking alterations, however, are in the vdw terms of the structures determined by NMR, which become large and negative for all systems, resulting in a favorable overall E_{pot}. These results show that some of the apparent instability of the NMR model structures may be attributed to differences between the force fields used to determine them and the GROMOS force fields used here. This is not a sufficient explanation, however, for the significantly less favorable total E_{pot} of the R-LTP2-N structure, even after minimization.

An alternative means of assessing the structures is to evaluate their quality using programs such as VADAR (*32*) or PROCHECK (*33*), which compare the values of a range of structural properties, such as dihedral angles, to the values expected based on analyses of databases of protein structures or calculations on small model systems. Each X-ray or NMR model structure of rice

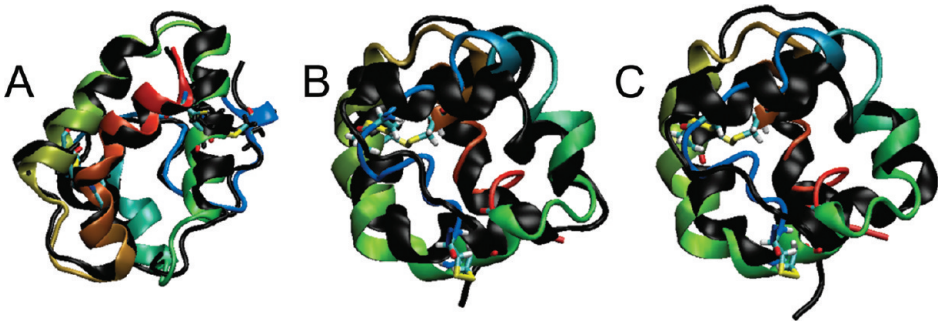

FIGURE 1: Overlaid structures of LTP1 and LTP2 from different sources. The backbone is shown as a cartoon, colored red at the N-terminus and blue at the C-terminus. The cysteine residues are shown as sticks and colored according to atom type. (A) LTP1: (rainbow) R-LTP1-X; (black) R-LTP1-N. (B) LTP2: (rainbow) R-LTP2-N; (black) W-LTP2-X. (C) LTP2: (rainbow) R-LTP2-N; (black) R-LTP2-H.

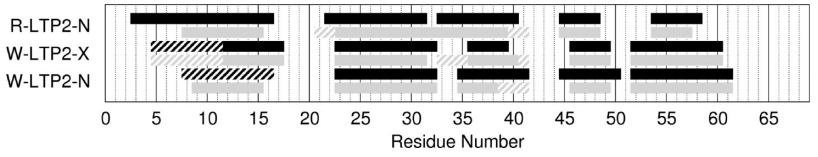

FIGURE 2: Plot showing the positions of the helices in the structures of rice and wheat LTP2 as labeled. α-Helices are shown by solid fill and 3_{10}-helices with checkered fill. The black bars correspond to the secondary structure classification made by the authors of each structure, and the gray bars show the secondary structure assigned by DSSP (*28*).

or wheat LTP2 was analyzed before and after minimization in the GROMOS 53A6 force field. As the majority of the properties that deviated most from the expected values did not change markedly upon minimization, only the results for the unminimized structures are discussed below.

Both VADAR and PROCHECK identified a significant number of residues with backbone ϕ/ψ angle values in unfavorable regions of the Ramachandran map, ω angle values that deviate substantially from 180°, and unfavorable combinations of χ_1/χ_2 angle values in the R-LTP2-N structure (Supporting Information Table S1, Figure S1, and Figure S5). There are also several nonideal bond lengths and bond angles and nonplanar aromatic systems. There is a larger concentration of residues exhibiting unfavorable ϕ/ψ and ω angles in the C-terminus of the protein, which is less structured in R-LTP2-N than in either of the wheat LTP2 structures (see below).

Only a few residues of W-LTP2-X exhibit unusual ω-angles or f_{VOL}; in all other respects, the structure conforms to the expected values, including the ASA and b_{VOL} (Supporting Information Table S1, Figure S2, and Figure S5). Simultaneous analysis of all model structures of W-LTP2-N revealed that only 75% of the residues have ϕ/ψ angles in the most favorable regions of the Ramachandran plot and that the side chains of many of the residues have unusual χ_1/χ_2 combinations and lower than expected f_{VOL} or vdw-based packing defects (Supporting Information Table S1, Figure S3, and Figure S5). Although W-LTP2-N is clearly not as favorable as W-LTP2-X according to VADAR and PROCHECK, it is still much more favorable than R-LTP2-N, reflecting the conclusions of the E_{pot} analysis.

Finally, the overall structure of R-LTP2-N was compared to W-LTP2-X and W-LTP2-N (Figure 1 and Supporting Information Table S2). As might be expected given the dissimilarity in sequence, the two wheat LTP2 structures are more like each other than R-LTP2-N. While there are slight differences in the orientation of the helices, the main difference is in the terminal helices. In Figure 2, the locations of the helices as reported along with the structures and as identified here according to DSSP (*28*) are compared for the three structures of LTP2. Different secondary structure classification procedures will obviously give slightly different results. For instance, the N-terminal helix of W-LTP2-N was originally classified as a 3_{10}-helix (*5*), whereas the DSSP analysis of this structure finds it to be a shorter α-helix. Although only the results for the first of the W-LTP2-N model structures are shown here, classification of the secondary structure of all nine models deposited in the PDB using DSSP revealed that only model 5 exhibits some 3_{10}-helix structure in the N-terminus, and only for residues 4, 9, and 10 (results not shown). Regardless, it is notable that for both the wheat and rice LTP2 NMR structures, and in particular for R-LTP2-N, the N-terminal helix is found here to be significantly shorter than its reported length. The C-terminal α-helix of R-LTP2-N is also significantly shorter than in the wheat LTP2 structures (Figure 2).

The absence of C-terminal α-helix in the R-LTP2-N structure may be because it is of the unliganded protein, whereas both W-LTP2-X and W-LTP2-N were solved with a lipid bound. Indeed, Hoh et al. (*7*) surmised that the hydrophobic cavity in which the ligand binds, which already differs between the X-ray and NMR wheat LTP2 structures, also changes upon lipid binding, describing the C-terminus (residues 56−67) of R-LTP2-N as having collapsed into the empty hydrophobic cavity. A similar observation has been made for LTP1, where in the apo form, residues 77−82 of the C-terminus loop point toward the hydrophobic cavity and block entry to the lipid-binding pocket. Binding of lipids to LTP1 also induces significant differences in the orientation of key ligand-binding residues (*34*). However in the SS-MD and DS-MD simulations discussed below, we do not see a loss of helical structure in the C-terminus of the other LTP2 structures, except at high temperatures, where the entire protein begins to unfold. Moreover, even if the unstructured nature of the C-terminus of R-LTP2-N is due to there being no ligand bound, this does not justify the unfavorable E_{pot}.

A further difference between the various structures of LTP2 noted by Hoh et al. (*7*) is the $C_\beta-S-S-C_\beta$ torsional angles. In both R-LTP2-N and W-LTP2-N these are far from the preferred values and have chiralities opposite to those in W-LTP2-X. Correspondingly, dihedral angles involving the sulfur atoms of

the cysteine residues constitute 122 of the 641 kJ·mol^{-1} proper dihedral angle energy of W-LTP2-N, 58 of the 841 kJ·mol^{-1} bond angle term of R-LTP2-N, and 54 of the 698 kJ·mol^{-1} proper dihedral term of R-LTP2-N. In comparison, they make up just 1 of the 873 kJ·mol^{-1} bond angle term and 16 of the 298 kJ·mol^{-1} proper dihedral term of W-LTP2-X. It seems, therefore, that the data and force fields used in the NMR structure determination procedures of both wheat and rice LTP2 were not sufficient to identify the correct disulfide bond conformations.

Overall, it seems reasonable to conclude that the main cause of the unfavorable E_{pot} of R-LTP2-N is problems with the structure determination procedure or with the NMR data. Fifteen conformers of R-LTP2 that "satisfied all of the constraints and possessed good nonbonded contacts" were determined (*4*), but only one was deposited in the PDB. The rmsd from the average structure was reported to be 0.154 nm for the backbone atoms of all residues, which is more than twice the 0.067 nm reported for the 10 structures determined for wheat LTP2 (*5*).

To test whether the R-LTP2 sequence is compatible with a better defined structure, a homology model was created based on the W-LTP2-X structure using the I-TASSER server (*23*). Initial assessment of the energy showed it to be extremely large and positive, particularly for the bond and vdw terms (Table 3). All energy terms other than the dihedral terms improved markedly upon energy minimization in either GROMOS force field. The low rmsd between the initial and minimized structures means that the high energies can be attributed to suboptimal local organization. The overall potential energy after minimization is comparable to that of minimized W-LTP2-X or W-LTP2-N and is substantially more favorable than that of R-LTP2-N. Additionally, analysis of this structure using VADAR and PROCHECK showed it to be much more favorable than R-LTP2-N (Supporting Information Table S1, Figure S4, and Figure S5), suggesting that the R-LTP2 sequence is not only compatible with but better suited to the more helical structure of W-LTP2.

It is of interest, therefore, to compare how well R-LTP2-N and R-LTP2-H fit the experimental data. Only the ^{1}H chemical shifts were deposited in the BMRB. The authors were able to provide the peak list (with intensities) of a ^{1}H−^{1}H NOESY spectrum, but with no information regarding how this raw data was processed into the NOE distances used in the refinement, it was impossible to attempt to replicate the restraint data. The proton chemical shifts were back-calculated using SHIFTX (*30*) from either the deposited R-LTP2-N or the R-LTP2-H structure created with I-TASSER. Hydrogens were added to the homology model using the program REDUCE (*31*). The unminimized structures were used because the minimizations were carried out in the GROMOS force field, in which aliphatic hydrogens are not explicitly represented. As the chemical shifts are predominantly determined by the chemical environment of a given atom, small differences in the positions assigned to the hydrogen atoms will not affect the calculated shifts significantly. The correspondence between the back-calculated and experimental ^{1}H shifts is almost identical for both structures, with a correlation coefficient of 0.97 (see Supporting Information Figure S6). The ^{1}H chemical shifts alone therefore do not contain sufficient information to define the correct structure of R-LTP2. This result is of importance with respect to the emergence of methods for calculating protein structures based solely on knowledge of the chemical shifts (*35*−*37*), although most use more than one type of chemical shift along with fragment replacement.

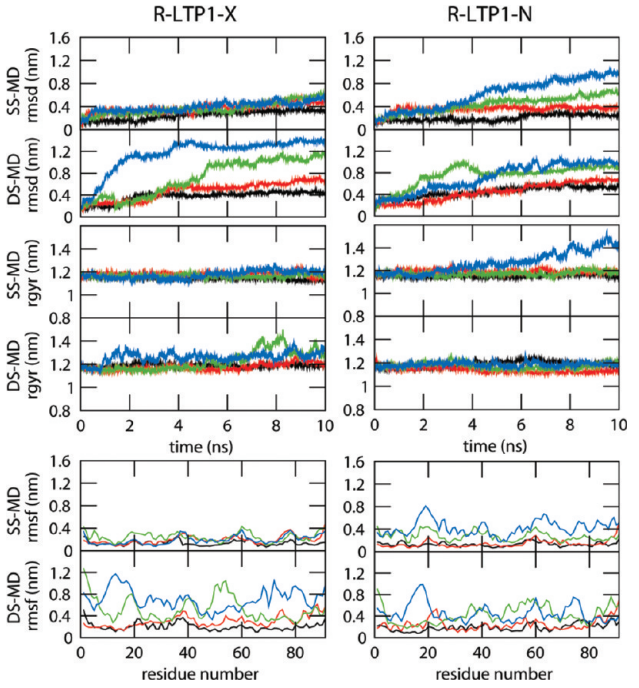

FIGURE 3: Time series of the atom-positional backbone rmsd from the energy-minimized starting structure, the r_{gyr}, and the C_α rmsf during SS-MD and DS-MD simulations of rice LTP1 starting from the X-ray or NMR model structure at four different simulation temperatures: (black) 298 K, (red) 328 K, (green) 348 K, and (blue) 373 K. For each type of analysis, the top row shows the results of the SS-MD and the lower row the results of the DS-MD.

Stability of LTP1 and LTP2 during MD Simulation. Given the above caveats about the integrity of the NMR model structures, particularly those of rice LTP2, the evolution of the structures during MD simulation is of interest. Both SS-MD and DS-MD were carried out with the GROMOS 53A6 force field at 298, 328, 348, and 373 K. The stability and behavior of each protein during the simulation were assessed by analyzing, for the backbone atoms of each protein, the root-mean-square-fluctuations (rmsf), the root-mean-square deviation (rmsd) with respect to the energy-minimized X-ray or NMR model structure, the radius of gyration (r_{gyr}), and the secondary structure. The 298 K simulations correspond to nondenaturing conditions, while 328 and 348 K are two of the temperatures used in the heat-denaturation disulfide-scrambling experiments of LTP1 and LTP2 (*16*). Simulations at 373 K were added to further explore the stability and because the disulfide shuffling is expected to increase at higher temperatures.

The structures solved by X-ray crystallography (R-LTP1-X and W-LTP2-X) behave much as might be expected during the simulations (Figure 3 and Figure 4). When the disulfide bonds are constrained, the rmsd increases initially and is then relatively constant throughout the simulation. The plateau rmsd is larger for higher temperatures. The temperature difference is more marked when the disulfide bonds are not constrained; in these simulations, the rmsd is particularly large at the highest temperatures, where the secondary structure is mostly lost (see also Figure 5 and Supporting Information Figure S7) and the r_{gyr} undergoes significant fluctuations. Otherwise, the r_{gyr} does not change markedly during the simulations except for in the SS-MD at 373 K, where it is slightly larger due to unravelling of the C-terminus. At low temperatures (298 and 328 K), there are small peaks in the rmsf in regions corresponding to turns and loops in

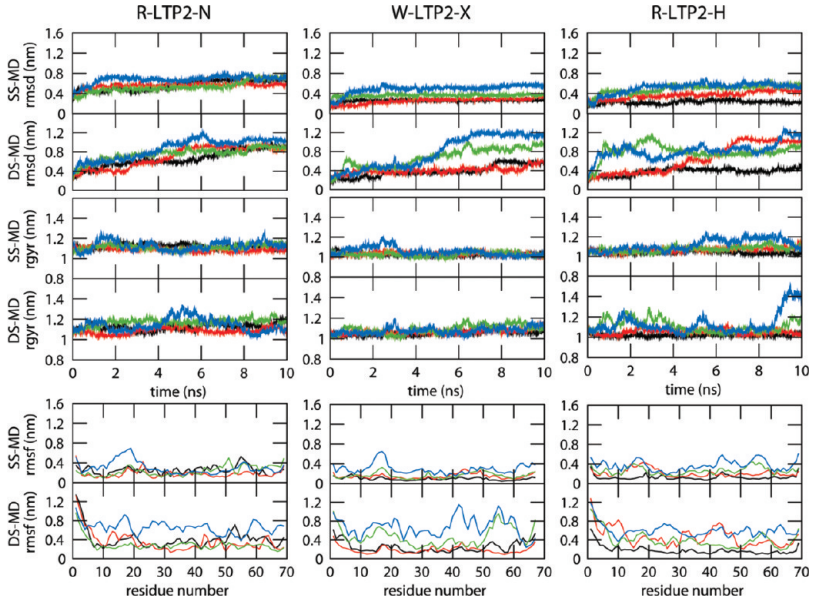

FIGURE 4: Time series of the atom-positional backbone rmsd from the energy-minimized starting structure, the rgyr and the C_α rmsf during SS-MD and DS-MD simulations of rice or wheat LTP2 starting from the NMR, X-ray or homology-modeled structure at four different simulation temperatures: (black) 298 K, (red) 328 K, (green) 348 K and (blue) 373 K. For each type of analysis, the top row shows the results of the SS-MD and the lower row the results of the DS-MD.

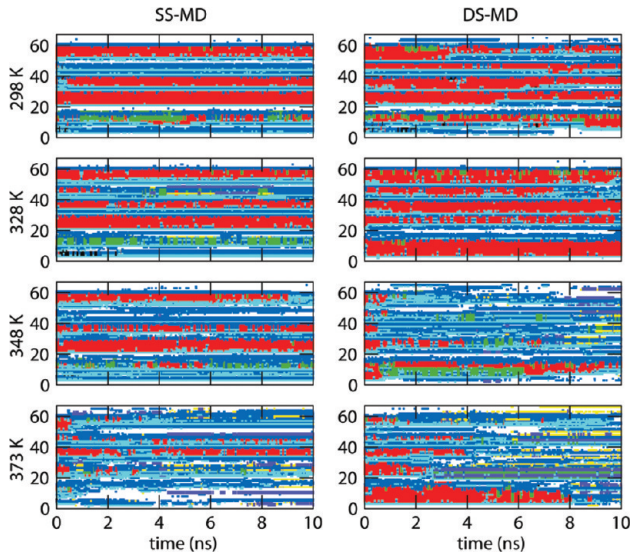

FIGURE 5: Time series of the secondary structure ((black) 3_{10}-helix, (red) α-helix, (green) π-helix, (blue) bend, (yellow) β-bridge, (violet) β-strand, and (cyan) turn) of W-LTP2-X during the SS-MD and DS-MD simulations at different temperatures as labeled.

the structure (residues 20, 38, 60, and 78 of R-LTP1-X and residues 17, 32, and 42−50 of W-LTP2-X); the structural fluctuations are concentrated here, and the helices remain relatively intact. Thus other than in the DS-MD at high temperatures, the secondary structure remains stable, with most deviation from the starting structure due to rearrangement of the secondary structure elements. The reduced stability in the high-temperature DS-MD simulations compared to the SS-MD simulations indicates that the disulfide bonds play a significant role in maintaining the structure of both R-LTP1 and W-LTP2.

R-LTP1-N, in comparison, behaves much the same with and without the disulfide bonds constrained, although other than at 373 K, the rmsd is marginally lower when the bonds are constrained. The large r_{gyr} of the 373 K SS-MD simulation is due to unwinding of the N-terminal helix (see Supporting Information Figure S8). This helix also dissolves in the 373 K DS-MD simulation but does not become displaced from the remainder of the structure. As with R-LTP1-X, most of the helical structure is lost in the DS-MD at 348 and 373 K, but in the other simulations it remains relatively intact, so that the large rmsd is due to rearrangement of the helices with respect to one another. In a further similarity, the peaks in the rmsf of the low-temperature SS-MD simulations correspond to loop regions (residues 20, 40, 60, and 78). Although the similar behavior in terms of rmsd in the SS-MD and DS-MD simulations might imply that the disulfide bonds are much less effective at maintaining the overall structure, the results of the other analyses suggest that the problem may be a suboptimal arrangement of the helices in the starting structure.

Although R-LTP2-N does show some differences in behavior depending on whether or not the disulfide bonds are constrained, overall, it is much less stable than R-LTP1-X, R-LTP1-N, and W-LTP2-X. The rmsd in the SS-MD simulations is significantly larger than that of W-LTP2-X and is similar (around 0.6−0.7 nm) at all temperatures. When the disulfide bonds are not constrained, the rmsd becomes larger than 0.8 nm at all temperatures. The r_{gyr} fluctuates considerably in all of the simulations and is also larger than that of W-LTP2-X. Like the rmsd, the rmsf is larger in magnitude than that of W-LTP2-X, particularly for the low-temperature simulations. The main peak in the rmsf of the 373 K SS-MD simulations is around residues 10−20, the same as for W-LTP2-X. What is most revealing is the secondary structure; little helical structure is maintained in any of the simulations, and in all but the 373 K SS-MD simulation, the helices that are present fluctuate between π- and α-helix (Figure 6).While the GROMOS 53A6 force field is known to be particularly poor at maintaining α-helices and often samples π-helices (*38*−*40*), the maintenance of the LTP1 and W-LTP2-X structures at all but the highest temperatures indicates that this is not the sole cause of the loss of structure of R-LTP2-N.

That the R-LTP2-N structure is inherently unstable is further highlighted by the behavior of the homology model (R-LTP2-H)

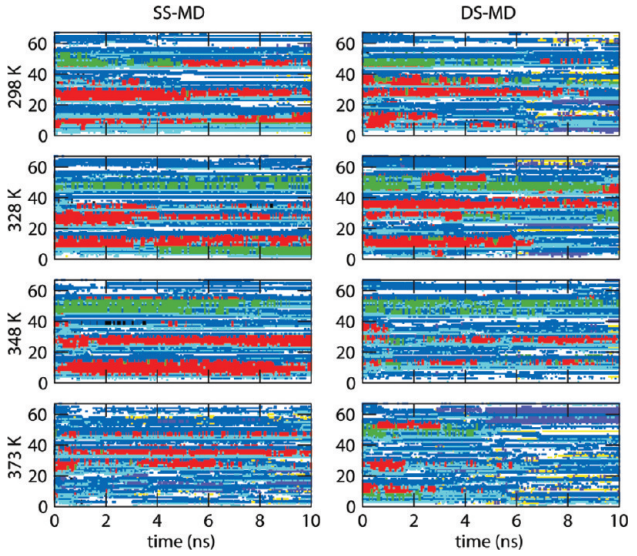

FIGURE 6: Time series of the secondary structure ((black) 3_{10}-helix, (red) α-helix, (green) π-helix, (blue) bend, (yellow) β-bridge, (violet) β-strand, and (cyan) turn) of R-LTP2-N during the SS-MD and DS-MD simulations at different temperatures as labeled.

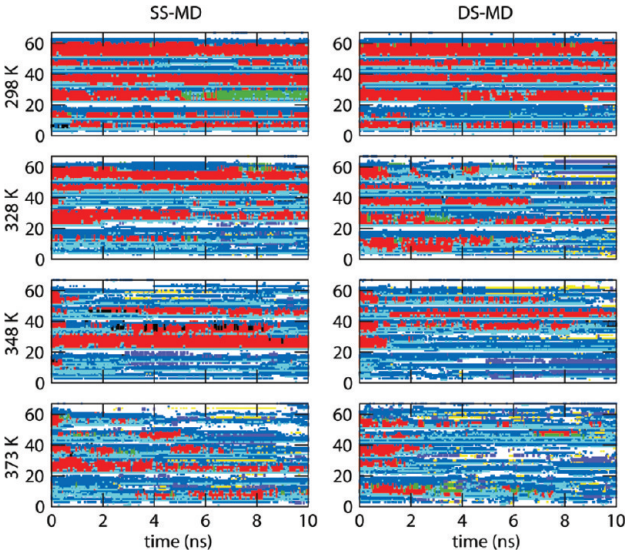

FIGURE 7: Time series of the secondary structure ((black) 3_{10}-helix, (red) α-helix, (green) π-helix, (blue) bend, (yellow) β-bridge, (violet) β-strand, and (cyan) turn) of R-LTP2-H during the SS-MD and DS-MD simulations at different temperatures as labeled.

(Figure 7). It shows temperature- and disulfide bond-dependent behavior similar to that of the X-ray structures, although the rmsd and rmsf at 328 and 348 K are somewhat larger than those of W-LTP2-X. The α-helical secondary structure is well maintained in both 298 K simulations and is mostly present in the higher temperature simulations, particularly at the beginning. While the helical structure of W-LTP2-X is slightly more stable, none of the LTP2 structures maintain their secondary structure as well as the LTP1 structures.

In the previous section, it was noted that the disorder of the C-terminus of R-LTP2-N might result from this structure having been solved without a ligand bound, in comparison to the other LTP2 structures, which were solved with lipids bound. No ligand was present in any of the simulations, but the α-helical structure of the C-terminus of W-LTP2-X and also R-LTP2-H is well maintained throughout the 298 K simulations, only disintegrating at higher temperatures when all of the helices become unstable. There is also no observable decrease in the r_{gyr}, ruling out collapse of a still-formed helix onto the remainder of the structure when the ligand is not present. Thus the MD simulations serve to further emphasize that there is something amiss with the rice LTP2 NMR model structure.

Disulfide Bond Shuffling. Disulfide bond shuffling during the unfolding and refolding of rice LTP1 and LTP2 has been studied experimentally (*16*), and a number of different scrambled isomers exhibiting different combinations of disulfide bonds were identified (Table 4). In the strong denaturants GdmCl and GdmSCN, more than 90% of the scrambled LTP1 isomers are of type a and b. In the presence of urea or when heat denatured, LTP1 also populates the type c and d partially folded intermediates. LTP2, in comparison, forms only one scrambled isomer (type a). In analyzing the simulations, a disulfide bond is defined to be present if the distance between the sulfur atoms of the two cysteine residues is less than 0.5 nm. The simulations of W-LTP2-X and R-LTP2-H were analyzed, even though W-LTP2-X has not been studied experimentally and R-LTP2-H is merely a predicted structure, to provide a point of comparison for the simulations of R-LTP2-N. The disulfide bond pattern for rice and wheat LTP2 is the same, but the residue numbering is slightly different. Only the results for the DS-MD simulations are shown; when the disulfide bonds are constrained, the bond length remains constant throughout the simulation, even at high temperature (data not shown).

Table 4: Disulfide-Bonded Residue Pairs of Native LTP1 and LTP2 and the Scrambled Isomers Identified by Lin et al.[a]

protein	type	disulfide bonded residues			
LTP1	native	3−50	13−27	28−73	48−87
	a	3−13	27−48	28−50	73−87
	b	3−13	27−28	48−50	73−87
	c	3−27	13−28	48−87	50−73
	d	3−13	27−28	48−87	50−73
LTP2	native	3−35	11−25	26−61	37−68
	a	3−11	25−26	35−37	61−68

[a]Reference *16*.

First, the state of the native disulfide bonds of LTP1 during the course of the simulations of R-LTP1-X and R-LTP1-N is examined (Figure 8). In the simulations of R-LTP1-X at 298 and 328 K, the native disulfide bonds remain formed for most of the simulation, other than those between residues 13−27, which separate after about 2 ns at 298 K, and between residues 48−87, which move apart after around 6 ns at 328 K. At 348 K, residues 13−27 and 28−73 are close together for the first half of the simulation, residues 48−87 separate near the start but come close again after 7 ns, and residues 3−50 become very far apart after 4 ns. At 373 K there is much fluctuation in the interresidue distances for all pairs, so that they are seldom close after the first few hundred picoseconds. When the simulations start from R-LTP1-N, all disulfide pairs remain close together at 298 K, although residues 3−50 move slightly further apart near the start and then maintain a similar separation throughout the simulation, and the distance between residues 28−73 increases a little after 4 ns. At 328 K, the distances between all native pairs of cysteine residues fluctuate, particularly in the final 5 ns. Although they do not always satisfy the definition of disulfide bond formation, the deviation is not large. At 348 and 373 K, however,

all pairs become separated within 1 or 5 ns, respectively, and do not come within 0.5 nm again. Overall, the behavior of the native disulfide bonds is similar for R-LTP1-X and R-LTP1-N. The progressive increase in the fluctuations and magnitude of the native sulfur−sulfur distances as the temperature is increased is in keeping with the increasing denaturation of the protein observed at higher temperatures, which was also seen experimentally (*16*).

The maintenance of the native disulfide bonds of W-LTP2-X and R-LTP2-H is also temperature-dependent (Figure 9). At 298 K, the distances are mostly less than or close to 0.5 nm, although there is more fluctuation at this temperature than for LTP1. The disulfide pairs involving the most terminal residues fluctuate the most, reflecting the greater disorder of the termini relative to the rest of the structure. As the temperature increases, the degree of fluctuation increases. Unlike for LTP1, the native disulfide pairs often move apart and then come together again several times during the simulation. In comparison to W-LTP2-X and R-LTP2-H, the native disulfide bonds of R-LTP2-N do not remain formed for the entire simulation at any temperature. The only exception is for residues 37−68 at 328 K. This behavior is in keeping with the poor retention of the R-LTP2-N structure in the DS-MD simulations.

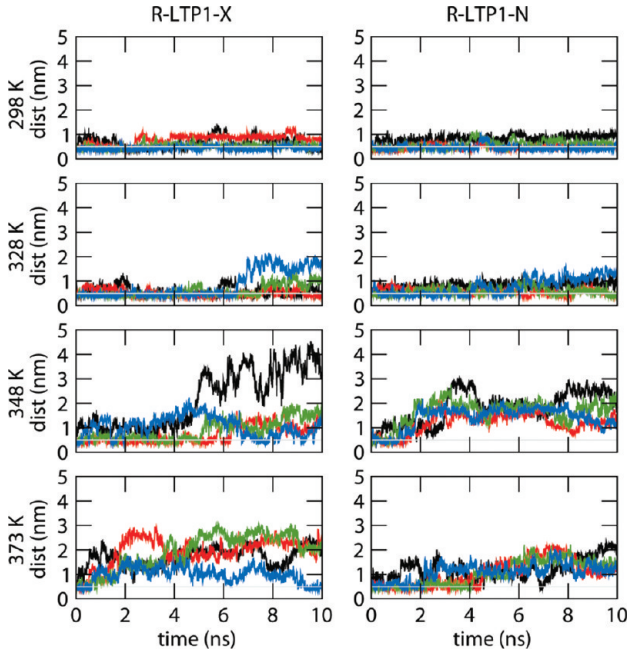

FIGURE 8: Time series of the sulfur−sulfur distances of the cysteine residues that form disulfide bonds in the native structures of rice LTP1 during DS-MD simulations starting from either R-LTP1-X or R-LTP1-N and at different temperatures as labeled. The residue pairs are colored according to (black) 3−50, (red) 13−27, (green) 28−73, and (blue) 48−87, and the gray line indicates 0.5 nm.

Overall, just as the rice and wheat LTP2 structures are not conserved as well as the rice LTP1 structures, with the least stable being R-LTP2-N, the native disulfide bonds of LTP2 do not perpetuate as well as those of LTP1 when they are not constrained, and R-LTP2-N again performs the worst. The similarity in the behavior of W-LTP2-X and R-LTP2-H and the maintenance of native disulfide distances close to 0.5 nm in the latter at 298 K show that the R-LTP2 sequence is compatible with a more helical structure such as those determined for wheat LTP2.

Next, the scrambled isomers (Table 4) identified in the disulfide-scrambling experiments (*16*) are considered to determine whether our simulations emulate the experimental results. None of the four scrambled isomers of rice LTP1 are fully formed at any point in the simulation of either R-LTP1-X or R-LTP1-N at any temperature (Figure 10 and Figure 11). In fact, of the disulfide pairs comprising set a, only residues 3−13 and 73−87 come close at all during the simulations, and only transiently; 3−13 at 373 K for R-LTP1-N and 73−87 at 348 K for R-LTP1-N and at 373 K for R-LTP1-X. For type b, as well as residues 73−87, residues 27−28 and 48−50 are also close to, but not less than, 0.5 nm apart throughout the simulations of both R-LTP1-X and R-LTP1-N. This is most likely due to their close sequence proximity, as a disulfide bond is unlikely to be able to form at such low sequence separation due to steric constraints. Indeed, these disulfide bonds were not actually identified experimentally: according to the description of the disulfide-scrambling methodology (*16*), short

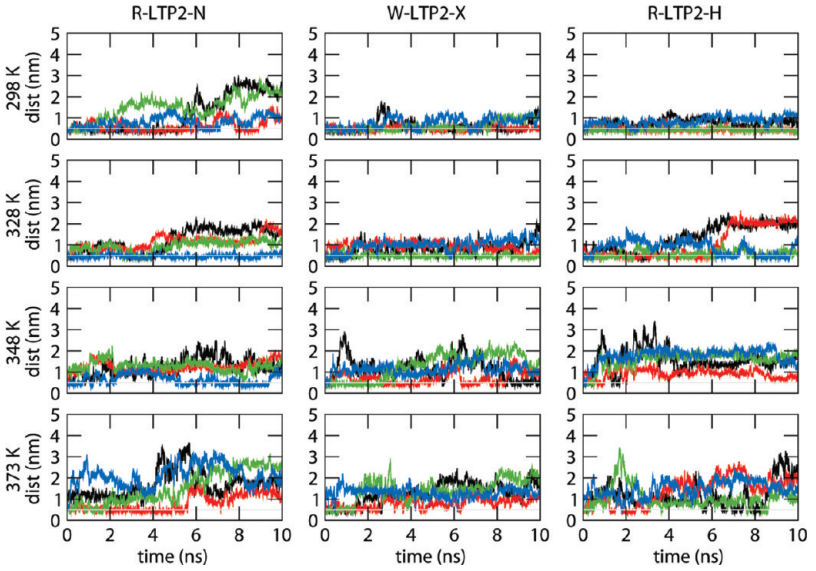

FIGURE 9: Time series of the sulfur−sulfur distances of the cysteine residues that form disulfide bonds in the native structures of rice or wheat LTP2 during DS-MD simulations starting from either R-LTP2-N, W-LTP2-X, or R-LTP2-H at different temperatures as labeled. The residue pairs are colored according to (black) 3−35 (2−34 for wheat LTP2), (red) 11−25 (10−24), (green) 26−61 (25−60), and (blue) 37−68 (36−67), and the gray line indicates 0.5 nm.

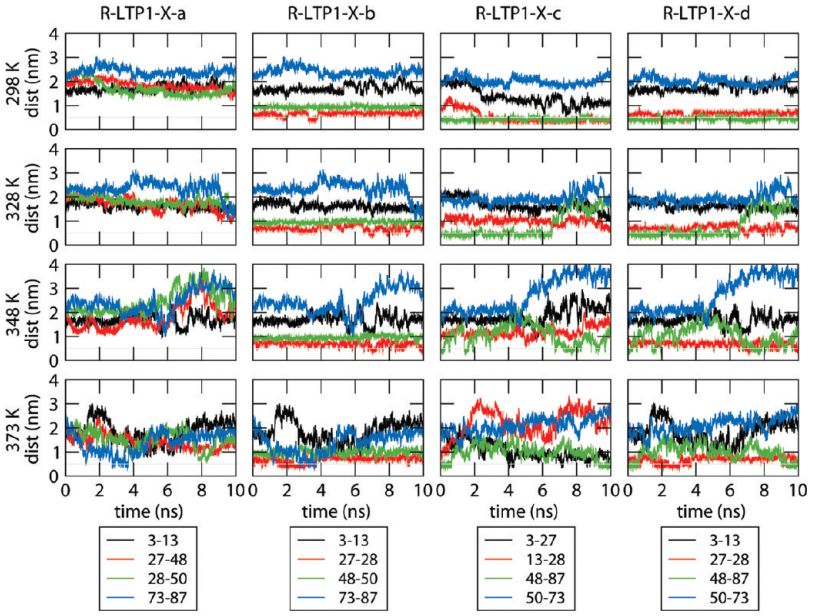

FIGURE 10: Time series of the sulfur−sulfur distances of the cysteine residues identified by Lin et al. (*16*) as forming disulfide bonds in the scrambled isomers of denatured rice LTP1 (Table 4) during DS-MD simulations of R-LTP1-X and R-LTP1-N at different temperatures as labeled. The residue pairs are colored as indicated in the figure legend, and the gray line indicates 0.5 nm.

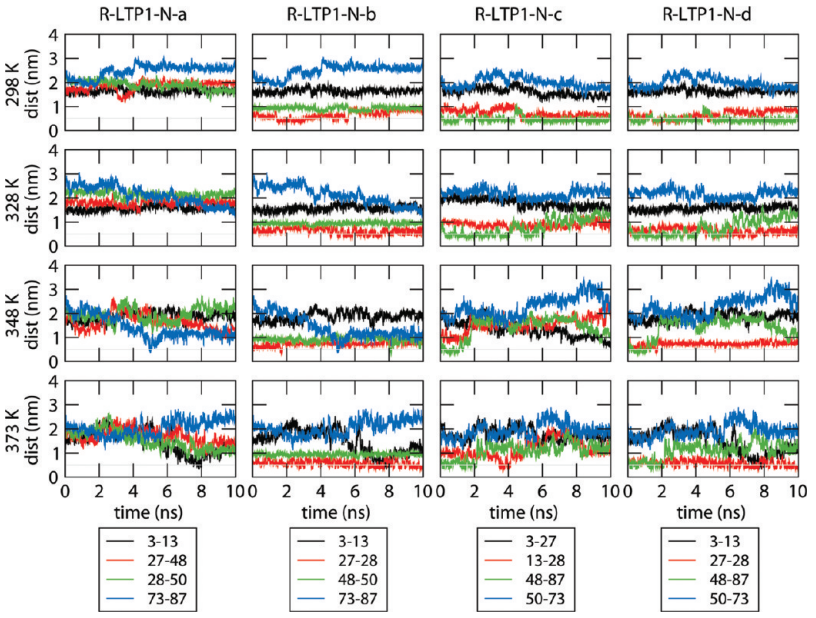

FIGURE 11: Time series of the sulfur−sulfur distances of the cysteine residues identified by Lin et al. (*16*) as forming disulfide bonds in the scrambled isomers of denatured rice LTP1 (Table 4) during DS-MD simulations of R-LTP1-X and R-LTP1-N at different temperatures as labeled. The residue pairs are colored as indicated in the figure legend, and the gray line indicates 0.5 nm.

peptides containing both of the residues concerned were isolated (after proteolytic degradation and HPLC), but the presence of a disulfide bond was not explicitly proven.

It appears initially that some of the disulfide bonds comprising the experimentally less populated isomers c and d are more likely to be formed by both R-LTP1-X and R-LTP1-N. Residues 48−87, in particular, are often close together. This is one of the native disulfide bonds, however, and thus is expected to be present, particularly at low temperatures, given that the simulations were started from the native structure. Of the non-native bonds, residues 13−28 are within 0.5 nm for the majority of the 298 K simulation of R-LTP1-X and for the initial part of all of the simulations of R-LTP1-N. This is probably due to a slight rearrangement of the helices relative to the initial structure, as residues 13−27 are natively bonded; only slight movement is then required to bring residues 13 and 28 close together. Thus out of all of the putative non-native pairings comprising the four scrambled isomers of LTP1, the only ones that actually occur are those that involve exchange of a disulfide bonding partner with a nearby residue. The pairs of residues near each other in sequence, such as 27−28, are of course also close together in space, but are unlikely to be able to attain the correct relative orientations for bond formation.

Only one scrambled isomer was identified experimentally for R-LTP2 (Figure 12). The residue pairings are all sequential, analogous to those of LTP1 type b. During the majority of the

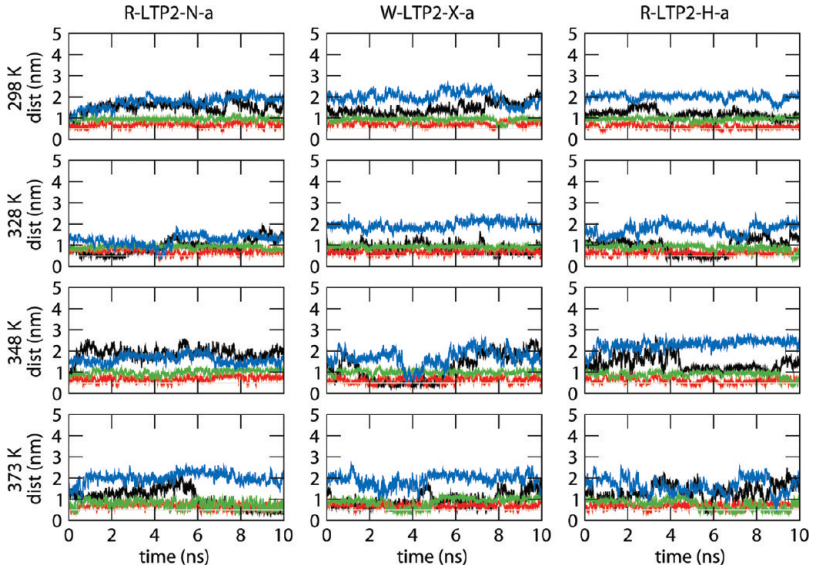

FIGURE 12: Time series of the sulfur−sulfur distances of the cysteine residues identified by Lin et al. (*16*) as forming disulfide bonds in the scrambled isomers of denatured rice LTP2 (Table 4) during DS-MD simulations of R-LTP2-N, W-LTP2-X, and R-LTP2-H at different temperatures as labeled. The residue pairs are colored according to (black) 3−11 (2−10 in wheat LTP2), (red) 25−26 (24−25), (green) 35−37 (34−36), and (blue) 61−68 (60−67), and the gray line indicates 0.5 nm.

simulations of R-LTP2-N, W-LTP2-X, and R-LTP2-H at all temperatures, residues 3−11 are close but not within 0.5 nm. Residues 25−26 and 35−37 are also close, but as for residues 27−28 in LTP1, this is most likely due to their sequence proximity. Only residues 61−68 are seldom close together, reflecting the generally disordered nature of the C-terminus in the DS-MD simulations. Similar to the results obtained for LTP1, all of the disulfide bonds of the LTP2 scrambled isomer are not simultaneously formed. Indeed, based on the short sequence separation of residues 25−26 and 35−37, it is doubtful whether they are all physically possible.

To investigate whether disulfide bonds other than those identified experimentally form during the simulations, the sulfur−sulfur distances between all possible pairs of cysteine residues were computed. Only those that are less than 0.5 nm for more than 10% of the simulation and do not occur in the native structure or in any of the scrambled isomers (Supporting Information Figure S9 and Figure S10) are discussed here.

For R-LTP1-X, only one disulfide pair fits these criteria: residues 27−73 are within 0.5 nm of each other more than 10% of the time at 328 and 348 K. More non-native bonds are observed for R-LTP1-N. Residues 13−73 are often close together at 298 and 328 K, as are residues 27−73 at 328 K. No non-native pairings are observed at 348 K, but at 373 K, residues 13−73 and 27−73 are again close together. The disulfide shuffling of residues 13, 27, and 73 is no doubt related to the native disulfide pattern of LTP1, in which residues 13−27 and 28−73 are bonded, so that only small alterations in the conformation are required to bring residues 13 and 27 close to residue 73.

More diverse combinations are seen for the LTP2 proteins. W-LTP2-X exhibits shuffling of its disulfide bonds at all temperatures. The closeness of residues 10−60 at 298 K can be linked to the native bonds between residues 10−24 and 25−60. Similarly, the short distance between residues 24−60 at 328 K can be linked to the native bond between residues 25−60. To bring residues 10−34 close together requires significant changes to the structure, however. When residues 2−10 and 2−24 are simultaneously close together at 348 K, the native bond between residues 10−24 is also present, such that the pair of residues involved in the bond is continuously shuffling. The near-identical distance between residues 24 and 25 and residue 34 during the 373 K simulation simply results from residues 24 and 25 being so close together in sequence. As the protein is mostly unfolded at this temperature, they are no longer constrained by the secondary structure to point in opposite directions. Of all the putative bonds identified for the LTP2 proteins, those between residues 2−10, 10−60, 24−34, and 25−34 are unique to W-LTP2-X, and the remainder, between residues 2−24, 10−34, and 24−60, also occur in the simulations of R-LTP2-N and R-LTP2-H. R-LTP2-N exhibits a further unique bond, between residues 11−68 at 348 K, whereas the potential bonds observed for R-LTP2-H are all seen in both R-LTP2-N and W-LTP2-X, albeit at different temperatures.

Experimentally, the folding mechanism and stability of LTP1 were found to be comparable to those of αLA (*16*). Investigation of αLA using disulfide-scrambling experiments (*11*, *12*) led to the identification of six well-populated scrambled isomers (*13*), but DS-MD simulations of bovine αLA (*17*) produced only one of the non-native bonds observed in the disulfide-shuffling experiments. This non-native disulfide bond was also observed in heat-denaturation experiments carried out without a thiol catalyst (*41*). Similarly, for LTP1 and LTP2, some of the non-native disulfide bonds were observed, but all four bonds characterizing a particular scrambled isomer were never observed simultaneously.

The differences between simulation and experiment may have various origins. Clear, neutralizing the cysteine residues and removing the disulfide bond constraint in a simulation are not sufficient to mimic the effect of a thiol catalyst in vitro, as while the bonds are effectively prebroken and the sulfur atoms do not repel each other, the bonds are not able to re-form. Second, any molecular model or force field has its limitations regarding accuracy, which may lead to incorrect structural predictions. A further explanation is the difference in time scales: the experiments take place over hours, whereas our simulations are many orders of magnitude shorter. Finally, the identification of particular disulfide bonds based on the experimental data is not

straightforward. Specifically, in all of the experimental disulfide-scrambling studies that have been carried out on a variety of different proteins, one of the identified scrambled isomers has the so-called beads-form pattern of disulfide bonds (*8*−*11*, *13*, *16*), in which the bonds are between consecutive cysteine residues. This isomer is in many cases the most common (*8*, *9*, *13*) and is generally associated with the most denaturing conditions (*10*, *11*). However, only for some proteins was it explicitly proven that such disulfide bonds are actually formed (*8*, *9*); for the others their formation was merely inferred from the presence of the two cysteine residues in the same peptide fragment. For some proteins, therefore, the beads-form isomer may in fact be a disordered state in which no disulfide bonds are formed.

CONCLUSIONS

Through simple energy calculations, structure quality assessment, structural comparisons, and, finally, comprehensive analysis of MD simulations, the NMR model structure of rice LTP2 deposited in the PDB was shown to be both energetically unfavorable and structurally unstable. In fact, all of the NMR model structures examined here were less stable than their counterparts solved by X-ray crystallography. The investigations were hampered, however, by unclear descriptions of the computational structure determination procedures, insufficient detail regarding which structure was deposited, and the omission of the secondary restraint data from the BMRB database. This result has profound importance given that the structures deposited in the PDB are widely used as the reference point for structural studies, including inferring structure−function relationships and initiating MD simulations, and for deriving knowledge-based statistical relationships. It is imperative, therefore, that the structures that are deposited are of the highest possible quality, are checked prior to submission, and come with sufficient meta information.

In the latter part of this work, a simple technique, in which the cysteine residues of a protein are neutralized to facilitate disulfide bond shuffling, was applied to investigate whether MD simulations can reproduce the disulfide bond shuffling observed experimentally for the rice LTP1 and LTP2 proteins. Some of the non-native disulfide bonds observed experimentally also occur in the simulations, but the specific combinations identified experimentally (*16*) are not seen. However, by comparing the simulations with and without the disulfide bonds constrained, the influence that the disulfide bonds have on the stability of each protein was able to be ascertained.

ACKNOWLEDGMENT

We are grateful to Lorna Smith for suggesting the project.

SUPPORTING INFORMATION AVAILABLE

A table of the rmsd between the different structures of LTP2 studied here, plots of the secondary structure of R-LTP1-X and R-LTP1-N, a scatter plot of the calculated and experimental ^{1}H chemical shifts, and a plot of the time series of the most populated non-native disulfide bonds that were not observed experimentally. This material is available free of charge via the Internet at http://pubs.acs.org.

REFERENCES

1. Kader, J.-C., Julienne, M., and Vergnolle, C. (1984) Purification and characterization of a spinach-leaf protein capable of transferring phospholipids from liposomes to mitochondria or chloroplasts. *Eur. Biophys. J. 139*, 411–416.
2. Kader, J.-C. (1996) Lipid-transfer proteins in plants. *Annu. Rev. Plant Physiol. Plant Mol. Biol. 47*, 627–654.
3. Kader, J.-C. (1997) Lipid-transfer proteins: a puzzling family of plant proteins. *Trends Plant Sci. 2*, 66–70.
4. Samuel, D., Liu, Y.-J., Cheng, C.-S., and Lyu, P.-C. (2002) Solution structure of plant nonspecific lipid transfer protein-2 from rice (*Oryza sativa*). *J. Biol. Chem. 277*, 35267–35273.
5. Pons, J.-L., de Lamotte, F., Gautier, M.-F., and Delsuc, M.-A. (2003) Refined solution structure of a liganded type 2 wheat nonspecific lipid transfer protein. *J. Biol. Chem. 278*, 14249–14256.
6. Charvolin, D., Douliez, J.-P., Marion, D., Cohen-Addad, C., and Pebay-Peyroula, E. (1999) The crystal structure of a wheat nonspecific lipid transfer protein (ns-LTP1) complexed with two molecules of phospholipid at 2.1 Å resolution. *Eur. J. Biochem. 264*, 562–568.
7. Hoh, F., Pons, J.-L., Gautier, M.-F., de Lamotte, F., and Dumas, C. (2005) Structure of a liganded type 2 nonspecific lipid-transfer protein from wheat and the molecular basis of lipid binding. *Acta Crystallogr. D 61*, 397–406.
8. Chang, J.-Y., Schindler, P., Ramseier, U., and Lai, P.-H. (1995) The disulfide folding pathway of human epidermal growth factor. *J. Biol. Chem. 270*, 9207–9216.
9. Chang, J.-Y., Schindler, P., and Chatrenet, B. (1995) The disulfide structures of scrambled hirudins. *J. Biol. Chem. 270*, 11992–11997.
10. Chang, J.-Y. (1999) Denatured states of tick anticoagulant peptide. Compositional analysis of unfolded scrambled isomers. *J. Biol. Chem. 274*, 123–128.
11. Chang, J.-Y., and Li, L. (2001) The structure of denatured α-lactalbumin elucidated by the technique of disulfide scrambling. Fractionation of conformational isomers of α-lactalbumin. *J. Biol. Chem. 276*, 9705–9712.
12. Chang, J.-Y. (2002) The folding pathway of α-lactalbumin elucidated by the technique of disulfide scrambling. Isolation of on-pathway and off-pathway intermediates. *J. Biol. Chem. 277*, 120–126.
13. Jui-Yoa, C., and Li, L. (2002) The unfolding mechanism and the disulfide structures of denatured lysozyme. *FEBS Lett. 511*, 73–78.
14. Salamanca, S., Villegas, V., Vendrell, J., Li, L., Aviles, F. X., and Chang, J.-Y. (2002) The unfolding pathway of leech carboxypeptidase inhibitor. *J. Biol. Chem. 277*, 17538–17543.
15. Singh, R. R., and Chang, J.-Y. (2004) Investigating conformational stability of bovine pancreatic phospholipase A2: a novel concept in evaluating the contribution of the "native-framework" of disulphides to the global conformational stability of proteins. *Biochem. J. 377*, 685–692.
16. Lin, C.-H., Li, L., Lyu, P.-C., and Chang, J.-Y. (2004) Distinct unfolding and refolding pathways of lipid transfer proteins LTP1 and LTP2. *Protein J. 23*, 553–566.
17. Schmid, N., Bolliger, C., Smith, L. J., and van Gunsteren, W. F. (2008) Disulfide bond shuffling in bovine α-lactalbumin: MD simulation confirms experiment. *Biochemistry 47*, 12104–12107.
18. Christen, M., Hünenberger, P. H., Bakowies, D., Baron, R., Bürgi, R., Geerke, D. P., Heinz, T. N., Kastenholz, M. A., Kräutler, V., Oostenbrink, C., Peter, C., Trzesniak, D., and van Gunsteren, W. F. (2005) The GROMOS software for biomolecular simulation: GROMOS05. *J. Comput. Chem. 26*, 1719–1751.
19. Oostenbrink, C., Villa, A., Mark, A. E., and van Gunsteren, W. F. (2004) A biomolecular force field based on the free enthalpy of hydration and solvation: The GROMOS force-field parameter sets 53A5 and 53A6. *J. Comput. Chem. 25*, 1656–1676.
20. Oostenbrink, C., Soares, T. A., van der Vegt, N. F. A., and van Gunsteren, W. F. (2005) Validation of the 53A6 GROMOS force field. *Eur. Biophys. J. 34*, 273–284.
21. Lee, J. Y., Min, K., Cha, H., Shin, D. H., Hwang, K. Y., and Suh, S. W. (1998) Rice nonspecific lipid transfer protein: the 1.6 Å crystal structure in the unliganded state reveals a small hydrophobic cavity. *J. Mol. Biol. 276*, 437–448.
22. Poznanski, J., Sodano, P., Suh, S. W., Lee, J. Y., Ptak, M., and Vovelle, F. (1999) Solution structure of a lipid transfer protein extracted from rice seeds. *Eur. J. Biochem. 259*, 692–708.
23. Zhang, Y. (2008) I-TASSER server for protein 3D structure prediction. *BMC Bioinf. 9*, 40.
24. Berendsen, H. J. C., Postma, J. P. M., van Gunsteren,W. F., and Hermans, J. (1981) in Intermolecular Forces (Pullmann, B., Ed.) pp 331−342, Reidel, Dordrecht, The Netherlands.
25. Ryckaert, J.-P., Ciccotti, G., and Berendsen, H. J. C. (1977) Numerical integration of the Cartesian equations of motion of a system with constraints: molecular dynamics of n-alkanes. *J. Comput. Phys. 23*, 327–341.

26. Berendsen, H. J. C., Postma, J. P. M., van Gunsteren, W. F., DiNola, A., and Haak, J. R. (1984) Molecular dynamics with coupling to an external bath. *J. Chem. Phys. 81*, 3684–3690.
27. Heinz, T. N., van Gunsteren, W. F., and Hünenberger, P. H. (2001) Comparison of four methods to compute the dielectric permittivity of liquids from molecular dynamics simulations. *J. Chem. Phys. 115*, 1125–1136.
28. Kabsch, W., and Sander, C. (1983) Dictionary of protein secondary structure: pattern recognition of hydrogen-bonded and geometrical features. *Biopolymers 22*, 2577–2637.
29. Humphrey, W., Dalke, A., and Schulten, K. (1996) VMD: Visual molecular dynamics. *J. Mol. Graphics 14*, 33–38.
30. Neal, S., Nip, A. M., Zhang, H., and Wishart, D. S. (2003) Rapid and accurate calculation of protein ^{1}H, ^{13}C and ^{15}N chemical shifts. *J. Biomol. NMR 26*, 215–240.
31. Word, J. M., Lovell, S. C., Richardson, J. S., and Richardson, D. C. (1999) Asparagine and glutamine: using hydrogen atom contacts in the choice of side-chain amide orientation. *J. Mol. Biol. 285*, 1735–1747.
32. Willard, L., Ranjan, A., Zhang, H., Monzavi, H., Boyko, R. F., Sykes, B. D., and Wishart, D. S. (2003) VADAR: a web server for quantitative evaluation of protein structure quality. *Nucleic Acids Res. 31*, 3316–3319.
33. Laskowski, R. A., MacArthur, M. W., Moss, D. S., and Thornton, J. M. (1993) PROCHECK—a program to check the stereochemical quality of protein structures. *J. Appl. Crystallogr. 26*, 283–291.
34. Cheng, H.-C., Cheng, P.-T., Peng, P., Lyu, P.-C., and Sun, Y.-J. (2004) Lipid binding in rice nonspecific lipid transfer protein-1 complexes from Oryza sativa. *Protein Sci. 13*, 2304–2315.
35. Cavalli, A., Salvatella, X., Dobson, C. M., and Vendruscolo, M. (2007) Protein structure determination from NMR chemical shifts. *Proc. Natl. Acad. Sci. U.S.A. 104*, 9615–9620.
36. Shen, Y.; et al. (2008) Consistent blind protein structure generation from NMR chemical shift data. *Proc. Natl. Acad. Sci. U.S.A. 105*, 4685–4690.
37. Vita, J. A., Ripoll, D. R., and Scheraga, H. A. (2007) Use of $^{13}C\alpha$ chemical shifts in protein structure determination. *J. Phys. Chem. B 111*, 6577–6585.
38. Cao, Z., Lin, Z., Wang, J., and Liu, H. (2008) Refining the description of peptide backbone conformations improves protein simulations using the GROMOS 53A6 force field. *J. Comput. Chem. 30*, 645–660.
39. Zagrovic, B., Gattin, Z., Lau, J., Huber, M., and van Gunsteren, W. (2008) Structure and dynamics of two β-peptides in solution from molecular dynamics simulations validated against experiment. *Eur. Biophys. J. 37*, 903–912.
40. Matthes, D., and de Groot, B. L. (2009) Secondary structure propensities in peptide folding simulations: a systematic comparison of molecular mechanics interaction schemes. *Biophys. J. 97*, 599–608.
41. Wijesinha-Bettoni, R., Gao, C., Jenkins, J. A., Mackie, A. R., Wilde, P. J., Mills, E. N. C., and Smith, L. J. (2007) Heat treatment of bovine α-lactalbumin results in partially folded, disulfide bond shuffled states with enhanced surface activity. *Biochemistry 46*, 9774–9784.